Influence of electron donors in fluorescent NLOphoric D-π-A derivatives with acenaphthene rotor: Photophysical, viscosity, and TD-DFT studies

Dhanraj R. Mohbiya, Ramnath R. Mallah, Nagaiyan Sekar*

Department of Dyestuff Technology, Institute of Chemical Technology, Matunga, Mumbai, 400 019, India

ABSTRACT

The novel fluorescent NLOphoric push-pull fluorophores (**2a-c**) constituted by the different N-substituted donors linked via π-bridge as a spacer to 1,1′-dicyanomethylidene group as an acceptor with acenaphthene rotor were synthesized and characterized. These dyes exhibit positive absorption and emission solvatochromism in solvents of different polarities. Solvent polarity plots viz. Lippert-Mataga, McRae, and Weller models provide the validation of charge transfer (CT) characteristics whereas, the Rettig model furnishes an alternative relaxation channel due to twisting around the σ-bonds between donor and acceptor on photoexcitation leading to the twisted intramolecular charge transfer (TICT) state in **2a-c**. Viscosity induced emission studies show 4.40, 8.78, and 5.63 fold increase in the emission intensity for dyes **2a**, **2b**, and **2c** respectively which recommends the titled dyes as a fluorescent molecular rotor (FMR). Density Functional Theory (DFT) calculations [(B3LYP/6-311++G(d,p)] give complete information of structural as well as electronic properties of dyes **2a-c**. The large difference in dipole moment (ca. 7.92–20.0 D) results in a strong non-linear optical (NLO) properties. The NLO properties were estimated theoretically as well as spectroscopically in solvents of different polarities. The computed values for these dyes show high first-order hyperpolarizability (β) in the range of $210–577 \times 10^{-3\circ}$ esu and second-order hyperpolarizability (γ) in the range of $506-2,325 \times 10^{-36}$ esu.

1. Introduction

In "push-pull" fluorophores, where an electron donor (D) and acceptor (A) moieties interact with the π-conjugated systems, a partial intramolecular charge transfer reaction takes place on photoexcitation [1]. The photophysics of donor-π-acceptor (D-π-A) compounds accompanied by photoinduced intramolecular charge transfer (ICT) is the focus of interest with respect to experimental as well as theoretical investigation [2–4]. The optical properties of such dyes are influenced by the factors such as viscosity, polarity, pH, voltage and the rigidity of the media [5]. Thus, to study such variations, many environment-sensitive dyes, have been reported [5–7]. These dyes can provide dynamic information about their surrounding stimuli by altering the fluorescence emission properties arises due to solvatochromism. Fluorescent molecular rotors (FMR) can be used to study such properties by using appropriate viscous media. Typically, FMRs have the ability to undergo intramolecular rotation around the σ-bonds between donor and acceptor on photoexcitation. Moreover, FMRs are utilized to measure the variations such as viscosity sensitivity, change in polarity and the non-linear optical (NLO) properties in the ground and excited state in different microenvironments.

A wide range of chemical functionalization or transformations of such D-π-A derivatives has been reported previously for their optical as well as non-linear optical (NLO) properties [8–12]. It is well documented that the optical and NLO properties of D-π-A derivatives can be fine-tuned by altering the donor or acceptor groups attached at the opposite end via the π-conjugated system. Moreover, these properties can be altered by using auxiliary donors or rotors (R) at the **α**-position with respect to 1,1′-dicyanomethylidene (DCMN) group as an acceptor [13]. A simple D-π-A derivative based on N-substituted donor and DCMN group as an acceptor have been reported for their excellent photophysical properties which have application in neuropathological fluorescence staining [14]. The optical properties of these derivatives are strongly influenced by varying the donors as well as the rotors attached at the **α**-position with respect to DCMN. A bathochromic shift in the absorption, as well as emission maxima, was observed while substituting the phenyl group at **α**-position with respect to DCMN [13]. On the other hand, the optical properties of these dyes further shifts to the red region while replacing the phenyl group with the strong acceptor such as cyano group (-CN) at **α**-position [15]. Consequently, further modification at the **α**-position with respect to DCMN group upon such derivatives makes us curious about the synthesis challenge and the

associated chemical and photophysical properties. In this context, we designated acenaphthene group as a rotor at the **α**-position with respect to DCMN group to examine the influence of different donors with respect to optical as well as NLO properties. Acenaphthene, a polycyclic aromatic hydrocarbon (PAH) containing functional derivatives have been investigated for quite some time, due to its planar structure as well as better spectral characteristics [16–25]. Despite the various synthetic strategies of acenaphthene derivatives, there are very few reports dealing with chemical functionalization or transformations of the compound accompanied by photophysical properties [26–31]. Acenaphthene based architecture is of importance for the functional applications such as organic electronics [32], fluorescent sensors [33], high-performance liquid chromatography [34], and various biological uses [31,35]. Consequently, the synthesis of specifically functionalized acenaphthene based architecture and their photophysical, as well as theoretical studies, are of considerable interest.

With these perspective, we have designed and synthesized three novel fluorescent NLOphoric D-π-A push-pull fluorophores containing acenaphthene as a rotor to study the influence of donors on linear as well as non-linear optical properties in solvents of different polarities. To get further insight into the electronic as well geometrical parameters of the dyes **2a-c**, DFT, and TD-DFT computations were carried out.

2. Experimental

2.1. Computational method

All the calculations were performed with the Gaussian 09 suite of the program [36]. The ground state geometry optimization of acenaphthene based D- π -A dyes **2a-c** were performed using Becke's three-parameter exchange Lee-Yang-Parr correlation functionals (B3LYP) with 6-311 + +G(d,p) basis set [37–41]. All the computations were performed on HP workstation XW 8600 with Xeon processor, 4 GB RAM, and Windows Vista as the operating system. TD-DFT computations were employed for excited state geometry optimization [42,43]. The polarizable continuum model (PCM) [44] as implemented in Gaussian 09 was used to optimize the ground and excited state geometries in solvents such as toluene (TOL), tetrahydrofuran (THF), chloroform (CHCl$_3$), ethyl acetate (EtOAc), acetone (ACE), acetonitrile (ACN), methanol (MeOH), and N,N-dimethylformamide (DMF). The excitation energies, oscillator strengths and orbital contribution for the lowest 20 singlet-singlet transitions at the optimized geometry in the ground state were obtained by TD-DFT calculations using the same basis set as for the geometry minimization in solvent environments. The NLO parameters were calculated using three different functionals - B3YPP, BHHLYP, and CAM-B3LYP - for comparison and the equations are as follow:

The total static dipole moment μ is expressed by the following equation

$$\mu = \sqrt{\mu_x^2 + \mu_y^2 + \mu_z^2} \tag{1}$$

The isotropic polarizability can be calculated from the trace of the polarization tensor,

$$\alpha_0 = \frac{(\alpha_{xx} + \alpha_{yy} + \alpha_{zz})}{3} \tag{2}$$

The mean first order hyperpolarizability (β_O) is expressed by

$$\beta_0 = (\beta_x^2 + \beta_y^2 + \beta_z^2)^{1/2} \tag{3}$$

$$\beta_0 = [(\beta_{xxx} + \beta_{xyy} + \beta_{xzz})^2 + (\beta_{yxx} + \beta_{yyy} + \beta_{yzz})^2 + (\beta_{zxx} + \beta_{zyy} + \beta_{zzz})^2]^{\frac{1}{2}} \tag{4}$$

Where, β_x, β_y, and β_z are the components of the second-order polarizability tensor along the x, y, and z-axes respectively.

The mean second order hyperpolarizability (γ) is expressed by

$$\gamma = \frac{1}{5}[(\gamma_{xxxx} + \gamma_{yyyy} + \gamma_{zzzz}) + 2(\gamma_{xxyy} + \gamma_{yyzz} + \gamma_{zzxx})] \tag{5}$$

2.2. Materials and equipment

All the chemicals are commercially available and were used without further purification unless otherwise mentioned. All the reagents were obtained from S. D. Fine Chemicals (India) and Sigma Aldrich. All the solvents used were of the spectroscopic grade. Melting points were recorded by open capillary on Sunder Industrial Product and are uncorrected. The reaction was monitored by thin layered chromatography (TLC) using 0.25 mm E-Merck silica gel 60 F254 precoated plates, which were visualized under UV light. ^{1}H NMR and ^{13}C NMR spectra were recorded on VARIAN 500-MHz instrument (USA) using CDCl$_3$ and DMSO-d$_6$ as a solvent. The chemical shifts were reported in parts per million (ppm) relative to internal standard as tetramethylsilane (TMS). ESI mass spectrometry was performed with a Q-TOF micromass (YA-105) spectrometer. Absorption spectra were recorded on Perkin Elmer Lambda 25 UV–vis spectrophotometer and emission spectra were recorded on Varian Inc. Cary Eclipse spectrofluorometer in the range 200–700 nm at room temperature. Cyclic voltammetry was performed on Metrohm autolab (AUT50995) with a standard three-electrode cell with a platinum electrode and an SCE reference.

2.3. Synthetic strategy

The energetic proximity of acenaphthene frontier orbital energy levels to those of N-substituted donor and DCMN as an acceptor based derivatives have motivated the synthesis of a variety of D-π-A conjugated heterocycles [45–48]. The synthesis of donor-acceptor compounds with the auxiliary effect of N-substituted phenyl ring at the **α**-position with respect to DCMN group has been reported previously [6,49–51]. In this report, we have designed and synthesized three different D-π-A derivatives based on N-substituted donor and DCMN group as an acceptor with an additional auxiliary effect of acenaphthene at the **α**-position to study the influence of different donors (Scheme 1) with respect to linear and NLO properties. These dyes were synthesized by Knoevenagel condensation of N, N-dimethyl phenylamine, julolidine, and triphenylamine based aldehydes with acenaphthene based active methylene compound (**1b**) to give the formation of three different D-π-A derivatives (Scheme 1).

2.4. Synthesis and characterization

The compounds **2a-c** were synthesized by modification of previously described methods [35,52,53]. Julolidine aldehyde and triphenyl monoaldehyde were synthesized by performing Vilsmeier-Haack reaction upon julolidine and triphenylamine respectively as described in the literature [50,54].

2.4.1. 5-Acetyl acenaphthene (*1a*)

Compound **1a** was synthesized as described in the literature [22].

2.4.2. 2-(1-(1,2-Dihydroacenaphthylen-5-yl)ethylidene)malononitrile (*1b*)

0.099 g (1.5 mmol) of malononitrile was added to the mixture of 0.196 g (1 mmol) of 5-acetylacenaphthene (**1a**) dissolved in 50 mL of glacial acetic acid. Ammonium acetate was added in a catalytic amount and the reaction mixture was stirred for 24 h at 90 °C. The reaction was monitored with the help of thin layer chromatography (TLC). After complete consumption of reactants, the reaction mixture was cooled to room temperature and poured over ice-cold water (50 mL) followed by extraction with the ethyl acetate. The organic layer was washed with water (3 x 20 mL) and brine, dried over sodium sulfate and evaporated under reduced pressure to give the crude product. The crude product was purified by column chromatography on silica 100–200 mesh using
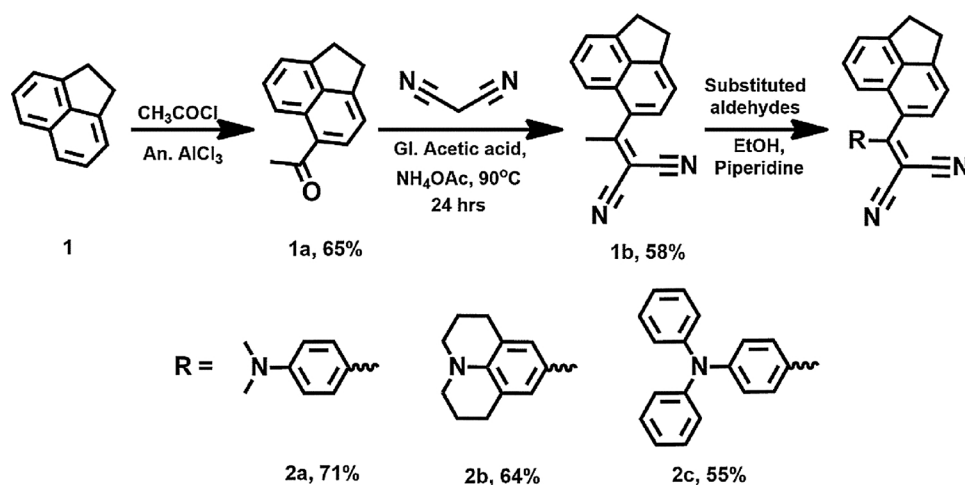
Scheme 1. The synthetic route for dyes 2a-c.

(9:1) hexane-ethyl acetate mixture as eluent.

Yield: 67%,

M.P.: 176-178 °C,

^{1}H NMR (500 MHz, CDCl$_3$) δ 7.58 (dd, J = 8.2, 7.1 Hz, 1 H), 7.42 (dd, J = 11.3, 7.7 Hz, 3 H), 7.35 (d, J = 7.2 Hz, 1 H), 3.45 (d, J = 2.3 Hz, 4 H), 2.77 (s, 3 H).

^{13}C NMR (125 MHz, CDCl$_3$) δ 177.46, 150.67, 147.13, 139.44, 129.88, 129.58, 127.56, 127.33, 120.64, 119.36, 118.76, 112.42, 112.23, 87.49, 30.44, 30.39, 25.48.

2.4.2.1. General procedure for the preparation of 2a-c. A mixture of either 0.244 g (1 mmol) of (**1b**) and substituted aldehydes (1 mmol) or 0.244 g (1 mmol) of (**1b**) and substituted aldehydes (1.5 mmol) was dissolved in absolute ethanol (50 mL). Piperidine was added in a catalytic amount (0.1 mL) and the reaction mixture was refluxed for 3 h. After complete consumption of reactants as indicated by TLC analysis, the excess solvent was removed under reduced pressure. The crude solid obtained was purified by column chromatography using silica gel 100–200 mesh and toluene as an eluent (Fig. 1).

2.4.3. (E)-2-(1-(1,2-Dihydroacenaphthylen-5-yl)-3-(4-(dimethylamino) phenyl) allylidene) malononitrile (2a)

The compound **2a** was prepared using the above general procedure from **1b** and *p*-dimethylaminobenzaldehyde. The greenish colored pure crystalline solid was obtained after silica gel column chromatography (100–200 mesh) in 78% yield.

M.P.: 192–194 °C,

^{1}**H NMR** (500 MHz, CDCl$_3$) δ 7.54 (d, J = 15.1 Hz, 1 H), 7.49 – 7.44 (m, 1 H), 7.39 (d, J = 8.2 Hz, 2 H), 7.37 – 7.33 (m, 4 H), 6.70 (d, J = 15.1 Hz, 1 H), 6.61 (d, J = 9.1 Hz, 2 H), 3.48 (s, 4 H), 3.05 (s, 6 H).

^{13}**C NMR** (125 MHz, CDCl$_3$) δ 171.08, 149.80, 149.14, 146.49, 139.30, 131.31, 129.26, 129.16, 128.96, 126.83, 120.15, 120.01, 119.36, 118.81, 114.37, 114.05, 111.81, 40.07, 30.44, 30.38.

MS (*m/z*): ((M + H)) 376.1858, Exact Mass: 375.1735.

2.4.4. (E)-2-(1-(1,2-Dihydroacenaphthylen-5-yl)-3-(1,2,3,5,6,7-hexahydropyrido[3,2,1-ij] quinolin-9-yl)allylidene)malononitrile (2b)

The compound **2b** was prepared using the above general procedure from **1b** and Julolidine-9-carbaldehyde. The navy blue colored pure solid was obtained after silica gel column chromatography (100–200 mesh) in 75% yield.

M.P.: 242–244 °C,

^{1}H NMR (500 MHz, CDCl$_3$) δ 7.45 (dd, J = 15.0, 6.7 Hz, 2 H), 7.37 (d, J = 8.8 Hz, 2 H), 7.33 (dd, J = 6.8, 4.7 Hz, 2 H), 6.92 (s, 2 H), 6.59 (d, J = 15.0 Hz, 1 H), 3.47 (s, 4 H), 3.30 – 3.24 (m, 4 H), 2.67 (t, J = 6.3 Hz, 4 H), 1.92 (dt, J = 12.1, 6.2 Hz, 4 H).

^{13}C NMR (125 MHz, CDCl$_3$) δ 170.82, 150.25, 148.86, 146.50, 146.38, 139.27, 129.34, 129.12, 129.04, 128.88, 127.20, 121.34, 121.17, 120.12, 120.03, 118.79, 118.05, 114.86, 114.60, 50.07, 30.44, 30.36, 27.48, 21.24.

MS (*m/z*): ((M + H)) 428.2164, Exact Mass: 427.2048.

2.4.5. (E)-2-(1-(1,2-Dihydroacenaphthylen-5-yl)-3-(4-(diphenylamino) phenyl) allylidene) malononitrile (2c)

The compound **2c** was prepared using the above general procedure from **1b** and 4-(diphenylamino)benzaldehyde. The orange-red colored pure crystalline solid was obtained after silica gel column chromatography (100–200 mesh) in 56% yield.

M.P.: 265–267 °C,

^{1}H NMR (500 MHz, CDCl$_3$) δ 7.58 (d, J = 15.3 Hz, 1 H), 7.48 (dd, J = 8.3, 6.9 Hz, 1 H), 7.42 – 7.34 (m, 4 H), 7.34 – 7.26 (m, 7 H), 7.16 – 7.08 (m, 5 H), 6.91 (d, J = 8.8 Hz, 2 H), 6.69 (d, J = 15.3 Hz, 1 H), 3.48 (s, 4 H).

^{13}C NMR (125 MHz, CDCl$_3$) δ 170.99, 151.16, 149.51, 148.71, 146.61, 146.18, 139.32, 130.41, 129.62, 129.30, 129.14, 129.04, 126.85, 125.89, 124.81, 121.57, 120.50, 120.29, 119.87, 118.85, 113.87, 113.51, 30.44, 30.41.

MS (*m/z*): ((M + H)) 500.2142, Exact Mass: 499.2048.
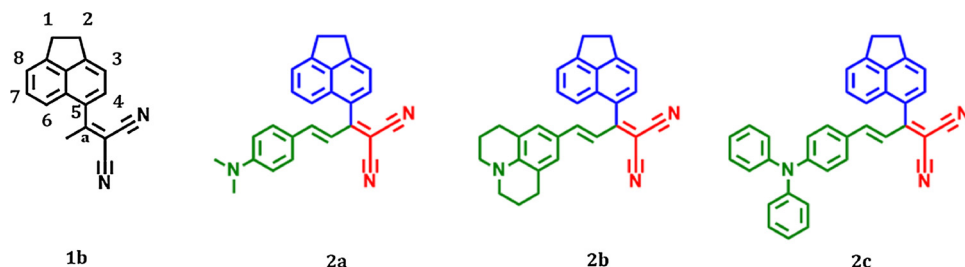
Fig. 1. The numbering scheme for acenaphthene and structure of synthesized dyes 2a-c.
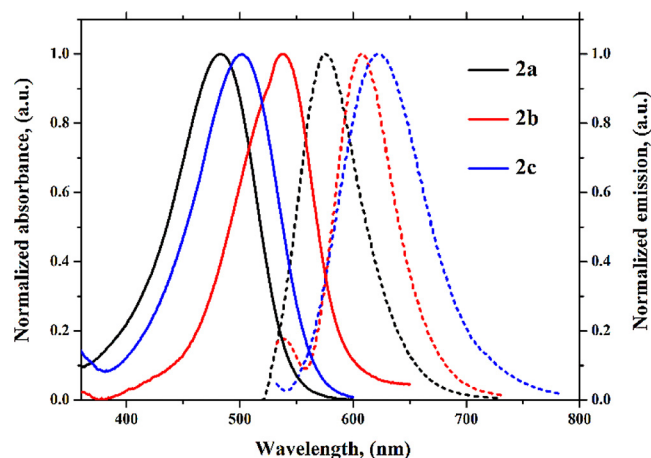
Fig. 2. Normalized absorption and emission graphs of 2a-c in chloroform.

3. Results and discussions

3.1. Photophysical properties

In order to study the solvatochromic behavior of the synthesized dyes (**2a-c**), absorption and emission spectra were taken in solvents of different polarity. Fig. 2 demonstrates the normalized absorption and emission graphs of **2a-c** in chloroform whereas Fig. S1 shows the absorption and emission graphs of **2a-c** in the different microenvironment. The photophysical properties such as absorption maxima, emission maxima, Stokes shift, molar extinction coefficient, full-width half maxima (FWHM) of the absorption band, oscillator strength and

fluorescence lifetime are summarized in Table 1. The synthesized dyes **2a-c** are of typical D-π-A chromophoric frameworks consisting of an electron donating N-alkyl/aryl unit and electron withdrawing DCMN unit. One of the main purposes of evaluating the photophysical properties of these dyes was to examine the effect of different electron donors along with acenaphthene group as an auxiliary rotor at **α**-position with respect to DCMN group as an acceptor. The UV–VIS absorption and emission spectra of the synthesized dyes **2a-c** were recorded at concentration 5×10^{-6} mol L^{-1}. From the photophysical data, it is seen that the absorption spectra of the dyes **2a-c** in chloroform show one intense broad band with onset at around 350–385 nm and a maximum centred at around 483 nm, 523 nm, and 482 nm respectively. This major absorption band can be assigned to the consolidated intramolecular charge transfer (ICT) transition, from N-substituted donor to DCMN acceptor center. In accordance with the characteristic behavior of ICT bands, the increase in electron donating character of styryl fragment causes a red shift of the absorption maxima (Fig. 2) in the order **2b** > **2c** > **2a**, whereas the Stokes shift calculated for the dyes follow the order **2c** > **2a** > **2b**. In donor-acceptor frameworks, planarity as well as steric hindrance play an important roles in enlarging the Stokes shift [55]. First, this effect causes the substituent to bend out of the main fluorophore plane in the ground state, which creates a prerequisite for this substituent to rotate in the excited state during geometry relaxation. Second, as the substituent rotates in the excited state, a strong interaction between the substituent and its adjacent atoms ensures that a large amount of torsional work is done, which is then translated into the Stokes shift. Among **2a-c**, the donors attached to **2a** and **2c** are freely rotating substituents which directly influences the planarity of the donor-acceptor framework. Conversely, in case of **2b** the donor-acceptor framework comprises planar structure due to julolidine group as a rigid donor. Thus, the major absorption band

Table 1
Observed photophysical parameters of dyes **2a-c** in solvents of different polarities.[a]

Dyes	Solvents	[b]λ_{abs} (nm)	[c]FWHM nm(cm^{-1})	[d]λ_{em} (nm)	[e]$\Delta\nu$ nm(cm^{-1})	[f]ε_{max} (mol^{-1}cm^{-1})	[g]f	[h]τ (ns)
2a	Toluene	487	73(3194)	551	64(2385)	42763	0.74	3.92
	THF	488	82(3511)	577	89(3161)	42750	0.76	5.20
	CHCl$_3$	483	82(3631)	568	85(3098)	56610	1.14	4.27
	EA	497	78(3283)	573	76(2669)	53469	0.97	4.98
	ACE	492	86(3640)	593	101(3462)	54828	1.14	3.84
	ACN	494	86(3610)	598	104(3521)	54144	1.02	2.25
	MeOH	496	86(3580)	593	97(3298)	64058	1.23	2.85
	DMF	505	86(3438)	606	101(3300)	43507	0.73	3.31
2b	Toluene	526	83(2979)	580	54(1770)	43346	0.67	4.48
	THF	527	92(3497)	602	75(2364)	34987	0.71	5.60
	EA	538	76(2720)	599	61(1893)	37015	0.59	6.68
	CHCl$_3$	523	79(2990)	600	77(2454)	34702	0.56	5.46
	ACE	535	83(2979)	619	84(2536)	43346	0.67	2.80
	ACN	540	85(3005)	622	82(2441)	43674	0.68	2.62
	MeOH	541	87(3066)	613	72(2171)	45555	0.81	1.63
	DMF	550	85(2895)	629	79(2284)	43891	0.66	2.67
2c	Toluene	493	85(3664)	577	84(2953)	50100	1.09	2.26
	THF	485	87(3783)	617	132(4411)	48235	0.96	3.50
	EA	502	84(3453)	615	113(3660)	48826	0.91	6.54
	CHCl$_3$	482	86(3843)	611	129(4380)	49910	1.01	3.01
	ACE	485	88(3835)	644	159(5091)	49603	0.98	1.04
	ACN	486	88(3819)	654	168(5286)	50338	0.96	1.22
	MeOH	490	90(3843)	552	62(2292)	48834	0.94	2.10
	DMF	493	94(3968)	652	159(4947)	50448	1.01	1.02

[a] Analysis was carried out at room temperature (25°C).

[b] Absorption maxima.

[c] Full-width half maxima of the absorption band.

[d] Emission maxima.

[e] Stokes Shift (nm) cm^{-1}.

[f] Molar extinction coefficient maxima (mol^{-1}cm^{-1}).

[g] Oscillator strength.

[h] Fluorescence lifetime (ns).

Table 2
Comparison of reported D-π-A framwork with the current work.

Rotors (R)	Donors (D)	Solvent	λ_{abs} (nm)	λ_{em} (nm)	β [ref.] (x 10^{-30} esu)	Ref.
H	H_3C-N-CH_3	CH_2Cl_2	433	487	73[1]	[14]
(benzene)	H_3C-N-CH_3	PBS(10 mM, pH 7.4)	484	647	–	[13]
CN	H_3C-N-CH_3	Acetone	582	–	–	[15]
(acenaphthene)	H_3C-N-CH_3	CHCl$_3$	483	568	308	This work
H	(julolidine)	CHCl$_3$	458	–	107 [1]	[55]
(acenaphthene)	(julolidine)	CHCl$_3$	523	600	347	This work
(acenaphthene)	(triphenylamine)	CHCl$_3$	482	611	616	This work

follows the order **2b > 2c > 2a** whereas, the increase in emission and the Stokes shifts as **2c > 2a > 2b**. This red-shifted absorption in **2b** can be attributed to + I effect of julolidine group, rigid planar framework, and conjugative delocalization in the ring from the donor (julolidine group) to the acceptor (DCMN group) end. Conversely, **2a** and **2c** showed a hypsochromic shift of lower degree around 483–505 nm as compared to **2b** due to free rotating alky and aryl group in **2a** and **2c** respectively. Dye **2b** show red-shifted absorption with an increase in solvent polarity that is from toluene (λ_{abs} 526 nm) to DMF (λ_{abs} 550 nm). Table 1 shows that the dye **2b** exhibits narrower absorption band with moderate ε_{max} values contrasted with that of the dyes **2a** and **2c**. Furthermore, we have compared the optical as well as NLO properties of some reported D-π-A framework with this work (Table 2). As can be seen from the Table 2, the optical properties of these dyes can be tuned by substituting the different donors or acceptors at the opposite end. Placing benzene ring at α-position with respect to DCMN causes red shifted absorption and emission property [13]. Moreover, the absorption band of the dyes further red shifted by replacing benzene ring with the strong electron acceptor –CN group [56]. Though optical properties of the dyes **2a-c** have not influenced dramatically by substituting the acenaphthene group at the **α**-position, their NLO properties were found to be superior to that of the reported D-π-A frameworks (Table 2). This must be due to non-centrosymmetry arising from acenaphthene group as rotor which enhances the non-linearity in dyes **2a-c** resulting in an improved NLO properties.

Moreover, the fluorescence emission spectra of the dyes **2a-c** show mirror image relationship (Fig. 2) with the broad emission bands relative to the corresponding absorption bands and are centered at around 551 nm to 664 nm. All the dyes reported in this work exhibited a slight red shift in emission maxima from non-polar to polar solvents. This outcome shows that these dyes exhibit positive solvatochromism, with continuous increment in the Stokes shift by increasing the solvent polarity. The calculated Stokes shift values, were found to be 3098, 2454, and 4380 cm^{-1} respectively for **2a-c**, which is an indication of

structural perturbations between the ground and excited state geometries. As can be seen from the Table 1, the Stokes shift of dyes increases in the order **2c > 2a > 2b**. There are substantial differences between the Stokes shifts of the dyes **2a, 2b and 2c** and these differences cannot be explained by the solvent effects. It is noted that the Stokes shifts of dye **2b** increases by only ~25 nm when a nonpolar solvent, such as toluene, is exchanged for the very polar DMF. In contrast, changes in the observed Stokes shifts are much larger with an alteration of donor groups from julolidine (**2b**) to the triphenylamine group (**2c**). The Stokes shift differences between **2b** and **2c** are as high as ~80 nm, even when compared in the same solvent (Table 1). Therefore, the Stokes shift differences among the dyes **2a-c** are more closely linked to the donors attached to the molecular framework. The larger Stokes shift values and the significant substituent effect on fluorescence revealed strong intramolecular charge transfer interactions between the N-substituted donor and DCMN as an acceptor. Such structural reorganization upon photoexcitation prompted us to screen the dyes under investigation for the FMR application.

3.2. Solvent polarity plots

The effect of synthesized dyes **2a-c** to solvent polarity can be perceived in terms of the difference in the dipole moments in the ground and excited states which can be assessed with the help of solvent polarity plots using Lippert-Mataga [59,60], McRae [61], Weller [62] and Rettigs [63,64] equation. The Lippert-Mataga and McRae plots depend on the polarity as well as the polarizability of the molecule and can be determined on the basis of Stokes shift of the molecules plotted against the orientation polarizability (Δf). On the contrary, the Weller and Rettig plots corresponds to the graph of emission maxima intensities (λ_{max}^{em}) in cm^{-1} versus the orientation polarizability (Δf) of the molecule. The calculated Stokes shift values, articulated in wavenumbers $\Delta\nu$ (cm^{-1}) = ($\nu_a - \nu_f$), is correlated with the solvent polarity or polarizability parameter (Δf) by the Eqs. (1) and (2), whereas the λ_{max}^{em} is correlated with the Δf by the Eqs. (3) and (4).

Equation (1)

$$\Delta\nu = m_1\Delta f_{LM} + constant$$
$$\Delta f_{LM} = \frac{\varepsilon - 1}{2\varepsilon + 1} - \frac{n^2 - 1}{2n^2 + 1}$$
$$m_1 = \left(\frac{1}{4\pi\varepsilon_0}\right)\frac{2(\mu_e - \mu_g)^2}{hca_0^3}$$
$$(\mu_e - \mu_g) = \sqrt{\frac{(4\pi\varepsilon_0)(hca_0^3)m_1}{2}} \tag{6}$$

Where, Δf_{LM} = orientation polarizability, m_1= Slope obtained from Lippert mataga plot h = Planck's constant, c = velocity of light in vacuum, a_0 = Onsager radii, μ_g = ground state dipole moment, μ_e = excited state dipole moment, ε_0 = permittivity of the vacuum,

Equation (2)

$$\Delta\nu = m_2\Delta f_{MR} + constant$$
$$\Delta f_{MR} = \left[\frac{(\varepsilon - 1)}{\varepsilon + 2} - \frac{(n^2 - 1)}{(n^2 + 2)}\right]$$
$$m_2 = \left(\frac{1}{4\pi\varepsilon_0}\right)\frac{2(\mu_e - \mu_g)^2}{hca_0^3}$$
$$(\mu_e - \mu_g) = \sqrt{\frac{(4\pi\varepsilon_0)(hca_0^3)m_2}{2}} \tag{7}$$

Equation (3)

$$\overline{v}f = \frac{2\mu_e^2}{hca^3}\Delta f_w + constant$$
$$\Delta f_w = \left(\frac{\varepsilon - 1}{2\varepsilon + 1} - \frac{1}{2}\frac{n^2 - 1}{2n^2 - 1}\right) \tag{8}$$
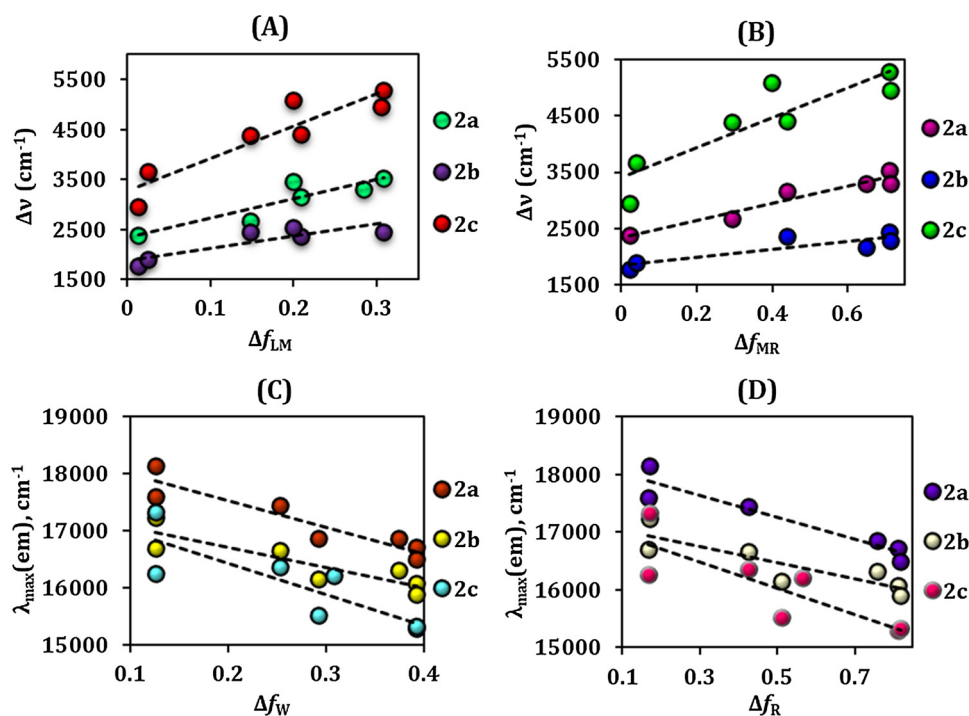
Equation (4)

Fig. 3. (A), (B) = the plot of $\Delta\nu$ versus Δf function according to Eqs. (S1), (S2). (C), (D) = λ_{max}(em),cm-1 versus Δf function according to Eqs. (S3), (S4). The line corresponds to the best linear fit to the data.

$$\bar{\nu}f = \frac{2\mu_e^2}{hca^3}\Delta f_R + constant$$

$$\Delta f_R = \left(\frac{\varepsilon - 1}{\varepsilon + 2} - \frac{n^2 - 1}{2n^2 - 4} \right) \tag{9}$$

By using these equations, the plot of $\Delta\nu$ versus Δf function as well as the plot of λ_{max}^{em} versus Δf function is obtained and is given in Fig. 3 and **S2-5** for dyes **2a-c**. From the graphs, a linear relationship is observed with the very good regression coefficient (close to unity) signifying the substantial charge transfer characteristics in synthesized dyes **2a-c**. The regression coefficient obtained for dyes **2a, 2b, and 2c** are 0.81, 0.75, and 0.84 respectively for Lippert-Mataga plot whereas, for McRae plot, the regression values were found to be 0.93, 0.77, and 0.79 respectively. Although the regression values are close to unity, it does not account for the order of charge transfer characteristics for synthesized dyes. The order of charge transfer characteristics in the synthesized dyes can be ascertained by the difference in the dipole moment ($\Delta\mu$) from ground (μ_g) to excited state (μ_e). The $\Delta\mu$ for all the dyes were calculated using the Eqs. (1) and (2), and the subsequent values are listed in Table S1. From the Table S1, it is seen that the $\Delta\mu$ for dyes **2c** was found to be largest as compared to other dyes. This large difference in the dipole moment from ground to excited state in dye **2c** is due triphenylamine group attached to the other end of the molecular framework. In dye **2c**, the rotating phenyl substituent is connected to the nitogen atom via a single bond. Its rotation during the geometry relaxation of the excited state can be explained by two competing effects. One is the effect of steric hindrance, causing it to bend out of the main fluorophore molecular plane; the other is the resonance effect, rendering a tendency to align with the molecular plane to achieve a better electron delocalization. Moreover, the charge transfer characteristic in the dyes **2a-c**, directly correlate to the Stokes shift. As can be seen from the Table 1, the charge transfer characteristics in dyes **2a-c** increases as the Stokes shift increases, **2c > 2a > 2b**. The synthesized dyes are also demonstrating the linear correlation as shown in the Rettigs plot (Fig. 3) which confirms that these dyes also exhibit considerable twisted intramolecular charge transfer (TICT). This substantial ICT and the TICT characteristics provoked us to examine the dyes **2a-c** for the FMR application.

3.3. Effect of solvent polarity on dipole moment of the ground and excited states

The solvent polarity dependent emission property can be expressed quantitatively conferring to the concept derived from the dielectric polarization [65], signifying that the spectral deviations of the fluorescence upon increasing the solvent polarity depend on the change in permanent dipole moments between ground (μ_g) and excited (μ_e) states. The deviations of dipole moment accompanied by ground and excited states, that is, $\Delta\mu = (\mu_e - \mu_g)$ was studied by the Eqs. (1) and (2) and summarized in Table S1. For dyes **2a-c**, Onsager radii (a_o) was evaluated to be 5.83, 6.13, and 6.33 Å respectively via B3LYP/6-311 + +G(d,p) level of theory. From the Table S1 it is observed that, for dyes **2a-c** the $\Delta\mu$ was found to be in the range of 3–13 Debye. On the other hand, dye **2c** was found to have the larger dipole moment difference as compared to **2a** and **2b**. As can be seen from the Table S1, the $\Delta\mu$ for dyes **2a-c** follows the order **2c > 2a > 2b**. This large difference in dipole moment for **2c** can be attributed to the larger perturbation of the molecular structure due to its free rotating phenyl as well as acenaphthene group attached at the donor and acceptor end, which makes the molecule vibronically disconcerted [55]. This major difference in dipole moment from ground to excited state favours the considerable intramolecular charge transfer within the dyes **2a-c**.

Furthermore, the change in dipole moment at excited state and ground state can be explained by using Bilot-Kawski function [66] which gives the ratio of ground and excited state dipole moment. The μ_g and μ_e values of a molecule can be determined by the solvent-polarity dependences of the absorption and fluorescence spectra on the basis of the simple quantum-mechanical second-order perturbation theory by Bilot-Kawski et al. by using the following solvent polarity parameters, $f_{BK}(\varepsilon, n)$ and $g_{BK}(\varepsilon, n)$ as follows,

$$f_{BK}(\varepsilon, n) = \frac{2n^2 + 1}{n^2 + 2}\left[\frac{\varepsilon - 1}{\varepsilon + 2} - \frac{n^2 - 1}{n^2 + 2} \right] \tag{10}$$

$$g_{BK}(\varepsilon, n) = \frac{3}{2}\frac{n^4 - 1}{(n^2 + 2)^2} \tag{11}$$

Where, ε = dielectric constant and n = refractive index

The slope m_1 is obtained by plotting the graph of $f_{BK}(\varepsilon, n)$ verses Stokes shift in cm^{-1} and slope m_2 is obtained by plotting graph of $f_{BK}(\varepsilon, n) + 2g(\varepsilon, n)$ verses $(\nu_a + \nu_f)$ cm^{-1}. The obtained parameters are summarized in Table S2 and the graphs are shown in **Fig. S6**. From these slope values m_1 and m_2, the ratio of excited state dipole moment to the ground state dipole moment was calculated. The final values of the ratio are summarized in Table S3. Interestingly, the ratio of dipole moment obtained by following the above mentioned equations display the same order as the order of Stokes shift as **2c** > **2a** > **2b**. We have also calculated ground state and excited state dipole moment and their ratio using B3LYP/6-311 + + G(d,p) and the data are listed in Table S4. The dipole moment ratio obtained for the dyes **2a**, **2b** and **2c** using computational method are greater than unity which confirms that the S_1 state are more polar as compared to S_0. Moreover, it is perceived that the dyes possessing large difference in the dipole moment are known to have significant non-linearity, thus synthesized dyes were further studied for the non-linear optical properties.

3.4. Viscosity sensitivity (FMR study)

As described earlier, the FMRs are the molecules which form TICT state upon photoexcitation due to intramolecular rotation around the σ-bonds between donor and acceptor core at the opposite end. Thus, to scrutinize the effect of the viscous environment towards acenaphthene and N-substituted donors rotating around the σ-bonds along with DCMN as an acceptor, we studied the sensitivity of all the dyes (**2a-c**) with the help of suitable viscous media as a function of FMR. Here, we have used polyethylene glycol (PEG) 400 system for the viscosity study, which is comparatively non-polar and commercially used viscous media as compared to a polar system like glycerol [67]. The measurements of viscosity sensitivity were conducted in binary mixtures of ethanol (EtOH) and polyethylene glycol (PEG) 400 system with viscosities that ranged from EtOH (100%): PEG 400(0%) to EtOH (0%): PEG 400 (100%). The dyes **2a-c** have less solubility in the mixture of EtOH and PEG 400 system. Therefore, these dyes have been solubilized in a highly polar aprotic solvent such as DCM and increased their viscosity using EtOH: PEG 400 system (Fig. 5). Interestingly, there is no red or blue shift in the emission maxima was observed as the viscosity increases, but the dyes **2a-c** show enhanced emission intensities by increasing the viscosity of the medium (Fig. 5). On the other hand, low-emission or non-radiative solutions are obtained at relatively low viscosities.

The emission intensity of the dyes **2a-c** and the viscosity of solvent was manifested with the help of Förster-Hoffmann Eq. (12).

$$\log I = x \log \eta + C \quad \text{.......} \quad (12)$$

where, I is the emission intensity of the dyes **2a-c**, η is the viscosity of the solvent, x is the viscosity sensitivity and C is constant. From the results (Fig. 5) it is seen that the dyes **2a-c** exhibit 4.40, 8.78, and 5.63 fold increase in the fluorescence emission intensity respectively. Accordingly, the double logarithmic plot of maxima emission intensities versus solvent viscosities was evaluated for the dyes **2a-c**. The graphs obtained were shown to have a good correlation between the emission intensity (I) of the dyes **2a-c** against the viscosity (η) of the solvent. Furthermore, the distinct color change was obtained from blue to red for all the dyes **2a-c** with the viscosity sensitivity (x) as, 0.32, 0.50, and 0.36 respectively (Figs. 4 and 5). From the graphs (Fig. 5), it is observed that the dye **2b** is found to have the better FMR activity as compared to **2a** and **2c** as well as the traditional FMR (DCVJ, x = 0.41) active compound [68]. This substantial increase in viscosity sensitivity of dye **2b** is due to the strong as well as rigid donor group (julolidine) attached via the π-conjugated system to the strong acceptor DCMN group. Form the above implications, it is evident that the dye **2b** shows the better FMR property with the distinct color change as compared to other dyes **2a, 2c** and DCVJ. We believe that such fluorescent dyes can be utilized
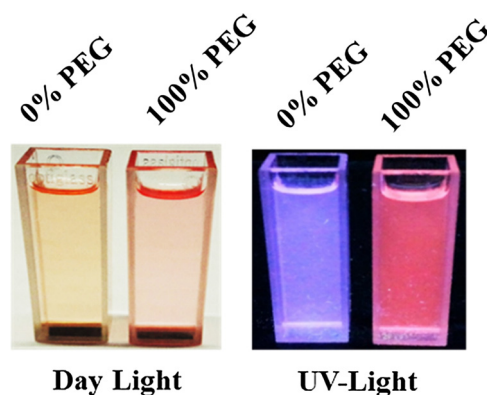
Fig. 4. Day Light and Uv-light photographs of dye 2b in 0% PEG +100% ethanol (blue color) and 100% PEG + 0% ethanol (red color) (For interpretation of the references to colour in this figure legend, the reader is referred to the web version of this article).

for the biological applications as all the dyes emit in the green region.

3.5. Cyclic voltammetry

The potentiodynamic electrochemical measurements of dyes **2a-c** were investigated with the help of cyclic voltammetry (CV). The measurements of CV plots were carried out using anhydrous ACN solutions containing 0.1 M tetrabutylammonium hexafluorophosphate (TBAPF6) as the supporting electrolyte. The reference electrode (Ag/Ag$^+$) was calibrated through the medium of ferrocene/ferrocenium (Fc/Fc$^+$) redox couple (4.8 eV below the vacuum level). Electrochemical potential obtained for dyes **2a-c** from the CV plot gives the evidence for HOMO-LUMO energy levels. The corresponding CV plots for dyes **2a-c** are given in Fig. 6 whereas the data related to HOMO and LUMO energy band gap is elucidated in Table 3. As shown in Fig. 6, CV plots of the dyes **2a-c**, each of these dye exhibits a reversible oxidation wave with the E_{onset}^{oxd} = 0.70 V, 0.72 V, and 0.73 V (vs. Ag/AgCl) respectively and reduction waves with E_{onset}^{red} = 0.65 V, 0.67 V, and 0.59 V (vs. Ag/AgCl) respectively. According to respective onset oxidation and reduction potentials, the HOMO and LUMO energies of dyes **2a-c** were evaluated (Table 3). The LUMO energies of dyes **2a-c** are around -2.91 eV, whereas the HOMO energies are slightly shifted towards the vacuum, *ca*. -5.10 eV (Table 3). This may be originated due to incorporation of more electron releasing groups as well as the elongation of the π-bridge of dyes **2a-c**. It is observed that the HOMO energies of these conjugated D-π-A dyes are lower than -5.3 eV which can improve their air-stabilities [69]. Moreover, the energies of HOMO are close to the work function of gold and hence can be endorse effective hole injection from the gold electrodes into the semiconducting layers [70].

3.6. DFT studies

3.6.1. Optimized geometries of dyes 2a-c

The optimized geometries of dyes **2a-c** in S_0 and S_1 state in chloroform are given in **Fig. S8** and the relative bond length, and dihedral angle are shown in Table S5. The bond lengths obtained from the optimized geometry of dyes **2a-c** at S_0 state are found to be almost similar as S_1 state. However, for dyes **2a-c** there is a slight decrease in bond length of C22-C11 from S_0 to S_1, whereas for **2c** there is an increase of 0.1 Å for bond C29-C28. Moreover, the consecutive increase and decrease in the bond length of the dyes **2a-c** suggest the charge transfer characteristics from donor to the acceptor. On the other hand, the dihedral angle obtained from the optimized geometry shows significant twisting from S_0 to S_1 state. For dyes **2a-c** the dihedral angle (C28-C22-C11-C10) was found to be 53.43°, 54.93°, and 52.63° respectively in S_0 state, whereas 45.42°, 41.15°, and 43.97° respectively in
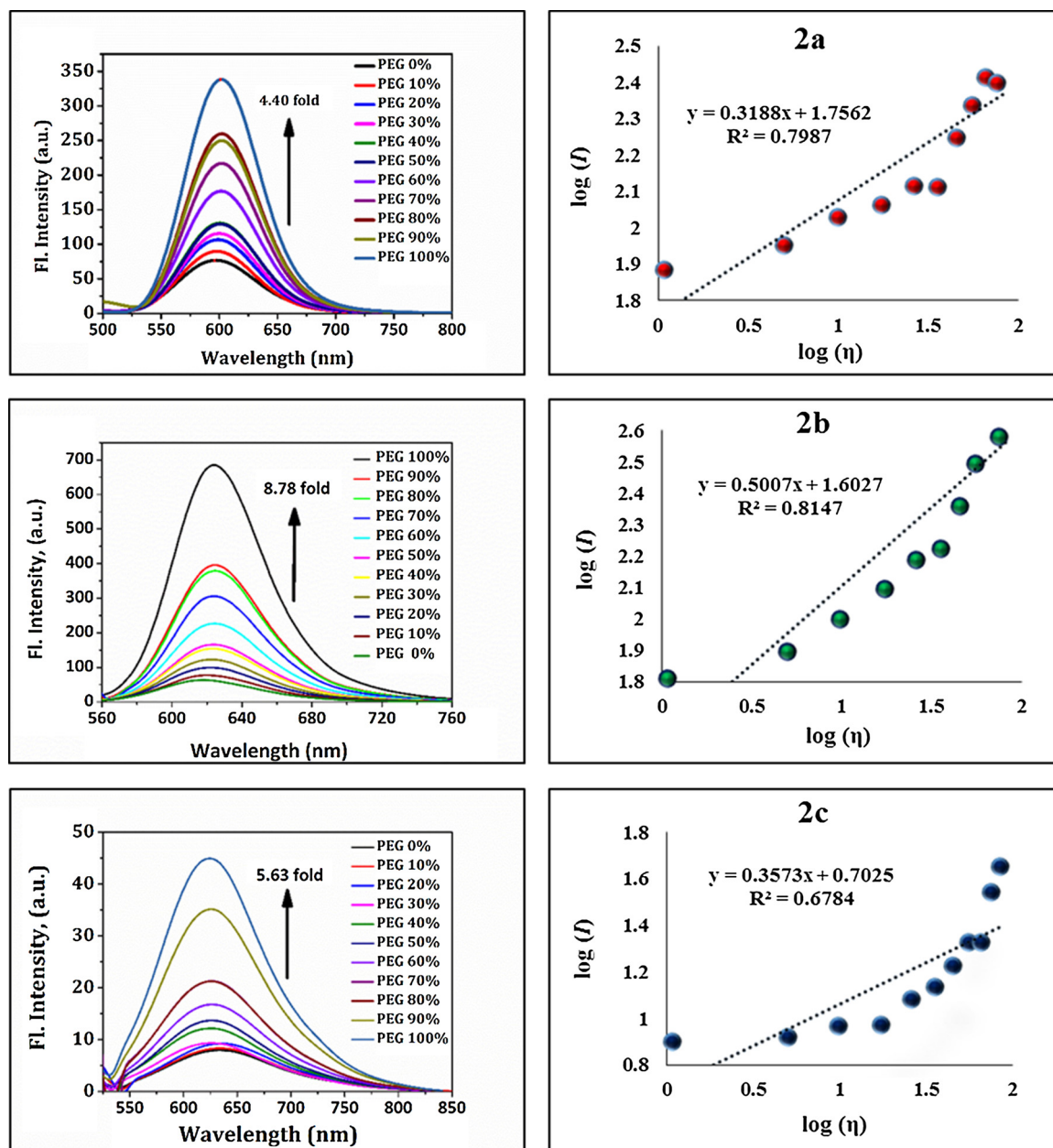
Fig. 5. Emission spectra of the dyes 2a-c in increasing amount of EtOH: PEG 400 system and the double logarithmic plot of maxima emission intensities versus solvent viscosities.
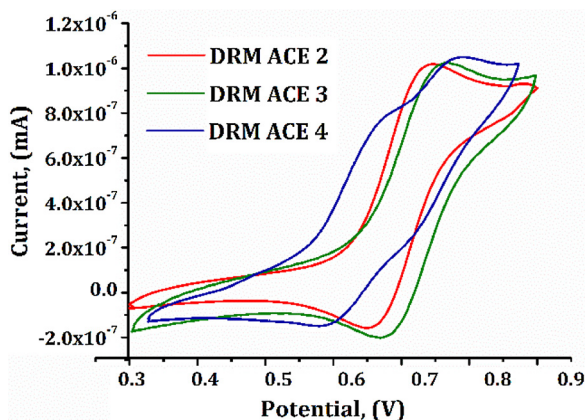
Fig. 6. Cyclic voltammograms of dyes 2a-c in acetonitrile.

S_1 state (**Table S5**). This pronounced twisting in the geometry of dyes **2a-c** is due to the intramolecular rotation of acenaphthene group around the σ-bonds attached at the α-position with respect to DCMN group. This twisting aspect of acenaphthene group in dyes **2a-c** can be attributed to the twisted intramolecular charge transfer (TICT) characteristics. Furthermore, the dihedral angle C31-C30-C29-C28 for dyes **2a-c** possesses the torsional change in the order of **2c** > **2a** > **2b** from S_0 to S_1 state. This outcome suggests that, as the dihedral angle increases, the Stokes shift of the dyes also increases in the order **2c** > **2a** > **2b**.

3.6.2. Electronic transitions (TD-DFT)

Theoretical predictions about the vertical excitation, oscillator strength, excitation energies and their orbital contributions for dyes **2a-c** are summarised in Table 4. The obtained data show that this transition in majority arises from an electron promotion from the highest occupied molecular orbital (HOMO) to the lowest unoccupied

Table 3

Electrochemical data for dyes 2a-c.

Dye	[a]λ_{onset} (nm)	[b]E_g	[c]E_{onset}^{oxd} (V)	[d]HOMO (eV)	[d]LUMO (eV)	[e]HOMO (eV)	[e]LUMO (eV)	[e]B.G. (eV)
2a	548	2.261	0.70	−5.071	−2.810	−8.256	−6.686	1.57
2b	600	2.071	0.72	−5.091	−3.020	−8.120	−6.664	1.46
2c	565	2.190	0.73	−5.100	−2.910	−8.341	−6.763	1.58

[a] λ_{onset} values are from absorption graphs in a $CHCl_3$ solvent.

[b] Optical band gap calculated from absorption onset/edge using reported equation [67].

[c] Values obtained from oxidation peak in CV plot.

[d] HOMO and LUMO level obtained from CV using reported equation [67].

[e] Theoretically calculated HOMO, LUMO, and band gap values from DFT calculations.

molecular orbital (LUMO). From the Table 4 it is observed that the estimated absorption and emission values calculated from the range separated functional (CAM-B3LYP) are in good agreement with the experimental data. While computing absorption wavelength, the least deviation of 6 nm for dye **2a** and the largest deviation of 13 nm for **2c** was observed. Similarly, for emission wavelength, the least deviation of 15 nm for **2a** whereas the largest deviations of 17 nm for **2c** was observed.

3.6.3. Frontier molecular orbitals (FMO) and molecular electrostatic potential surface (MEPS)

The qualitative indication of optical and electrical properties of the dyes and the association between geometric as well as the electronic structures can be derived from FMO. The electronic properties of D-π-A based conjugated dyes primarily depend on the energies of levels permissible for the electrons or holes as well as the energy band gap between these levels (i.e. HOMO and LUMO levels). The DFT computations [B3LYP/6-311 + +G(d,p)] were performed for the dyes **2a-c** to evaluate the energy levels of HOMO and LUMO used for the estimation of energy band gap between those conjugative levels. Fig. 7 illustrates the HOMO-LUMO energy levels along with the electronic charge distribution in the selected molecular orbitals for dyes **2a-c**. It is perceived that the first dipole-permissible electronic as well as resilient transition with the major oscillator strength, usually correspond almost exclusively from the elevation of an electron from HOMO to LUMO.

From the Fig. 7 it is observed that the electron density of the dyes **2a-c** in HOMO level largely located over the N-substituted donor part, whereas in the LUMO level the electron density largely shifted towards the DCMN part, with a small contribution from the phenyl ring of auxiliary donor (acenaphthene) part. Thus, N-alkyl/aryl part constitute donor state, while the DCMN part as an acceptor state. Compared to **2a** and **2c** the LUMO is more delocalized than HOMO in case of **2b**, signifying that the electron can easily move from donor to acceptor within the dyes which will facilitate enhanced charge transfer. This enhanced charge transfer can be attributed to the resilient electronic transition from HOMO to LUMO. Moreover, the electronic energy band gap
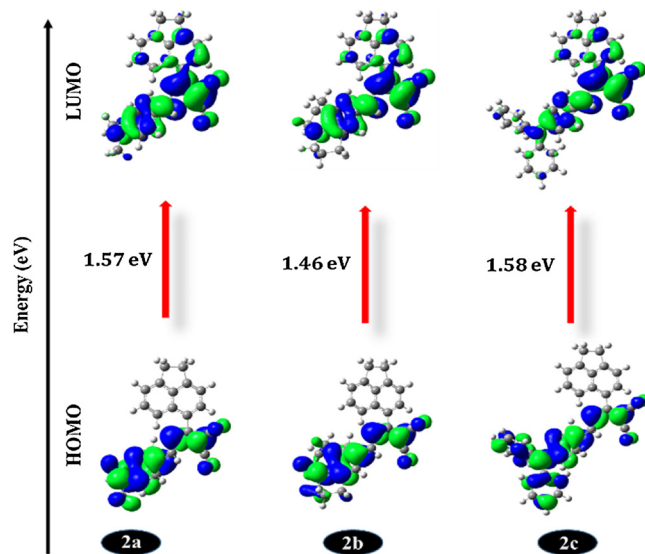
Fig. 7. Electronic distribution of the selected molecular orbitals for dyes 2a-c.

between HOMO to LUMO levels was found to be 1.57 eV, 1.46 eV, and 1.58 eV for dyes 2a-**c** respectively. This energy band gap further provisions the trend of charge transfer characteristics as described earlier for the dyes **2a-c** in the electrochemical data (Table 3). The energy band gap usually dependent on the substitution pattern of the donor-acceptor conjugated dyes. For example, if the donor-acceptor strength of the dyes increases, energy band gap decreases [72]. Thus, the minimization of energy band gap can be achieved by the proper substitution pattern of donor and acceptor groups for efficient charge transfer characteristics within the dyes. Furthermore, the charge transfer characteristics of the dyes **2a-c** were also supported with the help of MEPS contour plots (**Fig. S9**). It gives the qualitative indication of electrophilic or nucleophilic sites in the dyes by virtue of positive or negative

Table 4

Comparison of spectroscopically and computationally obtained absorption and emission parameters of dyes **2a-c** in chloroform.

Dye	λ_{abs}[a] (nm)	λ_{abs}[b] (nm)	f(E)[c] (eV)	T[d]	OC[e] (%)	λ_{ems}[f] (nm)	λ_{ems}[g] (nm)	f(E)[c] (eV)	T[d]	OC[e] (%)
2a	483	489	0.95(2.39)	H → L	91.94	568	553	0.96(2.25)	L → H	92.87
2b	523	531	1.09(2.31)	H → L	95.64	600	583	0.94(2.13)	L → H	98.30
2c	482	495	1.01(2.19)	H → L	95.43	611	595	0.95(2.19)	L → H	95.87

[a] Experimental absorption maxima in (nm).

[b] Theoretical absorption maxima in (nm).

[c] Oscillator strength with the excitation energy in (eV).

[d] Transition of the molecular orbitals.

[e] Orbital contribution in (%).

[f] Experimental emission maxima in (nm).

[g] Theoretical emission maxima in (nm).

electrostatic potential surfaces [73]. From the MEPS plots of dyes **2a-c**, it is observed that the DCMN part constitute negative electrostatic potential (red color), whereas N-substituted donor, as well as the auxiliary donor (acenaphthene) part, constitute positive electrostatic potential surface (blue color), as would be expected. From the above implications, it is seen that the dyes **2a-c** possess a strong electronic transfer from one side to the other, leading to enhanced ICT character within the dyes.

4. Polarizability and hyperpolarizabilities of 2a-c by spectroscopic and DFT methods

The D-π-A dyes are known to have very good non-linear optical (NLO) properties, due to which it has been used in many electronic as well as optoelectronic devices application [74]. The accurate estimation of polarizability and hyperpolarizability of the synthesized dyes (**2a-c**) are difficult, but in this paper we have made an attempt to comprehend the NLO responses of these types of D-π-A derivatives through spectroscopical as well as DFT methods and the resulting data are compared with that of urea which is a typical NLO material [75]. The spectroscopic NLO parameters such as transition dipole moment (μ_{CT}), linear polarizability (α_{CT}), first hyperpolarizability (β_{CT}) and second hyperpolarizability (γ_{SD}) were calculated using the reported method [76] and are presented in Table S6. Moreover, the theoretical NLO parameters such as onsager radii (a_0), static dipole moment (μ_0), mean polarizability (α_0), static first order hyperpolarizability (β_0) and second order hyperpolarizability (γ_0) for the dyes **2a-c** were calculated using three different functionals (B3LYP, BHHLYP, CAM-B3LYP) to compare the results obtained by the global hybrid (B3LYP, BHHLYP) and range-separated hybrid (CAM-B3LYP) functionals (Table S7). The complete theory employed for calculating the theoretical and experimental values for NLO properties are given in our previous reports [77–80].

4.1. Spectroscopic method

4.1.1. Polarizability and first order hyperpolarizability

The method we have used to determine the first polarizability (α_{CT} or α_{xx}) and second (β_{CT} or β_{xxx}) order hyperpolarizabilities of the dyes **2a-c**, is based on solvatochromism. The first polarizabilities α_{CT} or α_{xx} were calculated experimentally for the present fluorophores as described in the following equation [76],

$$\alpha_{CT} = \alpha_{xx} = 2\frac{\mu_{ge}^2}{E_{eg}} = \frac{2\mu_{eg}^2 \lambda_{eg}}{hc} \tag{13}$$

$$\mu_{eg}^2 = \frac{3e^2h}{8\pi^2 mc} \times \frac{f}{\bar{v}_{eg}} \tag{14}$$

where x is the direction of charge transfer, h is the Planks constant, c is the velocity of light in vacuum, λ_{eg} is the wavelength of transition from the ground state to excited state, $\bar{v}_{eg}$ is the absorption frequency μ_{ge} is the transition dipole moment respectively. Thus, obtained results for linear polarizability α_{CT}, the oscillator strength (f) and the transition dipole moment (μ_{ge}) of dyes **2a-c** are tabulated in Table S6. The observed values of α_{CT} are higher in polar solvent environment (DMF) in the range of 38.73–49.4355×10^{-24} e.s.u.while lower in case of non-polar solvent environment (toluene) 22.40–31.10×10^{-24} e.s.u. for all dyes.

The two-level microscopic model used to determine solvent dependent hyperpolarizability is based on Oudar and Chemla equation [58,81] which in modified form can be presented as,

$$\beta_{xxx} = \beta_{CT} = \frac{3v_{eg}^2 \Delta\mu_{CT}}{2h^2 c^2 (v_{eg}^2 - v_L^2)(v_{eg}^2 - 4v_L^2)} \tag{15}$$

where x, h, c, μ_{eg} is described above in Eq. (13), v_{eg} is the transition frequency, v_L is the frequency of the reference incident radiation, $\Delta\mu_{CT}$

is the difference between dipole moments of the ground state and excited state which is taken from McRae's theory. β_{xxx} is the dominant tensor component of the first hyperpolarizability and as the formula refers to charge transfer transition, the results obtained by this equation is often indicated as β_{CT} (charge transfer). When there is no laser excitation ($v_L = 0$) and we get the results of static hyperpolarizability. Therefore, Eq. (13) reduces to the following equation:

$$\beta_{CT} = \beta_{xxx} = \frac{3\mu_{eg}^2 \Delta\mu_{CT}}{2E_{eg}^2} \tag{16}$$

The results of the first hyperpolarizability (β_{CT}) obtained using the solvatochromic method are tabulated in Table S6. The results of β_{CT} using two-level model depend on the several assumptions and a rough approximation of leading tensor of entire first hyperpolarizability along the way of charge transfer through π-conjugation as well as the space dipole moments distribution which has a major influence to the results of β_{CT} [82]. The values of quadratic hyperpolarizability ($\mu\beta_{CT}$) for the hybrid dyes are 571.23×10^{-48} esu (**2a**), 612.14×10^{-48} esu (**2b**), and 862.15×10^{-48} esu (**2c**) in DMF. These values are highly influenced by the solvent polarity and show higher values in a more polar solvent (DMF) compared to non-polar solvent (toluene).

4.1.2. Second order hyperpolarizability (γ)

The second-order hyperpolarizability is also termed as solvatochromic descriptor $< \gamma >_{SD}$ which is formulated from the electronic polarization in the non-resonant region at the molecular level can be treated by a three-level model [83,84] using the density matrix formalism given in the Eq. (15),

$$\gamma_{xxxx} \propto \frac{1}{E_{ge}^3}\mu_{ge}^2(\Delta\mu_{eg}^2 - \mu_{ge}^2) \tag{17}$$

The calculated "solvatochromic descriptor" for the second order hyperpolarizability values for synthesized dyes in toluene and DMF solvents are given in Table S6. The values of $\langle\gamma\rangle_{SD}$ for all the dyes are; 67.84×10^{-36} (**2a**), 66.55×10^{-36} (**2b**), and 60.13×10^{-36} (**2c**) in DMF respectively.

4.2. Theoretical method

Here, we have elucidated the NLO parameters of spectroscopically obtained data with the theoretical one for comparison. In this regard, the NLO properties of the synthesized dyes were estimated with respect to the global hybrid (GH) as well as the range separated hybrid (RSH) functionals using the standard triple zeta basis set, 6-311 + + G(d,p). The results obtained by both the methods GH and RSH were found to be in good agreement with each other (Table S7). The polarizability and hyperpolarizability values obtained for dyes **2a-c** were found to be solvent dependent. The NLO responses of the particular dye can be tailored by changing the transition dipole moment [85,86]. From the Table S6–S7, it can be seen that the increase in solvent polarity is responsible for enhanced molecular hyperpolarizability of the dyes **2a-c**. Moreover, the polarizability and hyperpolarizability values vary according to the donor and acceptor strength of the dyes. The theoretically derived values of α, β and γ for dyes **2a-c** were found to be in range 70–111×10^{-24} esu, 210–577×10^{-30} esu, and 506-$2,325 \times 10^{-36}$ esu respectively (Table S6–S7). These values were compared with that of urea ($\alpha_{urea} = 6.2 \times 10^{-24}$ e.s.u., $\beta_{urea} = 0.31 \times 10^{-30}$ e.s.u., $\gamma_{urea} = 4.46 \times 10^{-36}$ e.s.u.) which was found to be larger than that of urea, indicating the enhanced NLO properties in dyes **2a-c**. Moreover, the β values of these dyes were compared with the reported donor-acceptor acetylenes [87] as well as polyenes [57] and found to be superier than that of reported dyes. In particular, the NLO properties of the dyes are mainly rely on the length of π-conjugation as well as the strength of the donor and acceptor moiety. Such high NLO properties can be endorsed the targeted dyes for optoelectronic device

applications.

5. Conclusion

In summary, we have successfully designed and synthesized novel acenaphthene based D-π-A derivatives with N-substituted donors and DCMN as an acceptor. All the dyes showed positive solvatochromism from non-polar (toluene) to polar (DMF) environment. The polarity plots drawn on the basis of Lippert-Mataga, McRae and Weller model confer reasonable sign of charge transfer characteristics whereas, the Rettig model furnishes TICT state for dyes **2a-c** which is been used for the FMR application. Among all the dyes, **2b** was found to have the higher viscosity sensitivity (x = 0.50) as compared to other dyes as well as traditional FMR (DCVJ, x = 0.41) dye. The DFT calculations reported here deliver a significantly increased fundamental understanding of dyes **2a-c**. On the other hand, the polarizability and hyperpolarizability values estimated for dyes **2a-c** were found be superior than that of urea which makes the dyes suitable for the non-linear optical materials.

Appendix A. Supplementary data

Supplementary material related to this article can be found, in the online version, at doi:https://doi.org/10.1016/j.jphotochem.2018.05.039.

References

[1] M. Blanchard-Desce, R. Wortmann, S. Lebus, J.M. Lehn, P. Krämer, Intramolecular charge transfer in elongated donor-acceptor conjugated polyenes, Chem. Phys. Lett. 243 (1995) 526–532, http://dx.doi.org/10.1016/0009-2614(95)00895-B.

[2] A. Wiessner, W. Ku, T. Fiebig, H. Staerk, Intramolecular charge transfer (ICT) and solvation of a rigidly linked pyrene / N-methylindolino derivative and related compounds in linear alcohols, J. Phys. Chem. A 101 (1997) 350–359, http://dx.doi.org/10.1021/jp961182f.

[3] K.G. Thorat, A.K. Ray, N. Sekar, Modulating TICT to ICT characteristics of acid switchable red emitting boradiazaindacene chromophores: perspectives from synthesis, photophysical, hyperpolarizability and TD-DFT studies, Dye Pigm. 136 (2017) 321–334, http://dx.doi.org/10.1016/j.dyepig.2016.08.049.

[4] S.I. Druzhinin, S.A. Kovalenko, T. Senyushkina, K.A. Zachariasse, Dynamics of ultrafast intramolecular charge transfer with 1-tert-butyl-6-cyano-1,2,3,4-tetrahydroquinoline (NTC6) in n-hexane and acetonitrile, J. Phys. Chem. A 111 (2007) 12878–12890, http://dx.doi.org/10.1021/jp074983z.

[5] L.S. Kocsis, K.M. Elbel, B.A. Hardigree, K.M. Brummond, M.A. Haidekker, E.A. Theodorakis, Cyclopenta[b]naphthalene cyanoacrylate dyes: synthesis and evaluation as fluorescent molecular rotors, Org. Biomol. Chem. 13 (2015) 2965–2973, http://dx.doi.org/10.1039/C4OB02563F.

[6] R.D. Telore, M.A. Satam, N. Sekar, Push-pull fluorophores with viscosity dependent and aggregation induced emissions insensitive to polarity, Dye Pigm. 122 (2015) 359–367, http://dx.doi.org/10.1016/j.dyepig.2015.07.017.

[7] H. Qian, M.E. Cousins, E.H. Horak, A. Wakefield, M.D. Liptak, I. Aprahamian, Suppression of Kasha's rule as a mechanism for fluorescent molecular rotors and aggregation-induced emission, Nat. Chem. 9 (2017) 83–87, http://dx.doi.org/10.1038/nchem.2612.

[8] S. Mohamed, D. Demeter, J.-A. Laffitte, P. Blanchard, J. Roncali, Structure-properties relationships in triarylamine-based donor-acceptor molecules containing naphtyl groups as donor material for organic solar cells, Sci. Rep. 5 (2015) 9031, http://dx.doi.org/10.1038/srep09031.

[9] Y. Wang, C. Shu, E.M. Breitung, R.J. Mcmahon, Synthesis and characterization of thiazole-containing chromophores for second-order nonlinear optics, J. Mater. Chem. 9 (1999) 1449–1452, http://dx.doi.org/10.1039/A900820I.

[10] K.Y. Suponitsky, Y. Liao, A.E. Masunov, Electronic hyperpolarizabilities for donor-acceptor molecules with long conjugated bridges: calculations versus experiment, J. Phys. Chem. A 113 (2009) 10994–11001, http://dx.doi.org/10.1021/jp902293q.

[11] M. Damaceanu, C. Constantin, L. Marin, Insights into the effect of donor-acceptor strength modulation on physical properties of phenoxazine-based imine dyes, Dye Pigm. 134 (2016) 382–396.

[12] P.K. Nandi, N. Panja, T.K. Ghanty, Heterocycle-based isomeric chromophores with substantially varying NLO properties: a new structure-property correlation study, J. Phys. Chem. A 112 (2008) 4844–4852, http://dx.doi.org/10.1021/jp710010f.

[13] T. Zhu, J. Du, W. Cao, J. Fan, X. Peng, Microenvironment-sensitive fluorescent dyes for recognition of serum albumin in urine and imaging in living cells, Ind. Eng. Chem. Res. 55 (2016) 527–533, http://dx.doi.org/10.1021/acs.iecr.5b04214.

[14] M. Cui, M. Ono, H. Watanabe, H. Kimura, B. Liu, H. Saji, Smart near-infrared fluorescence probes with donor-acceptor structure for in vivo detection of β-amyloid deposits, J. Am. Chem. Soc. 136 (2014) 3388–3394, http://dx.doi.org/10.1021/ja4052922.

[15] F. Tancini, Y.-L. Wu, W.B. Schweizer, J.-P. Gisselbrecht, C. Boudon, P.D. Jarowski, M.T. Beels, I. Biaggio, F. Diederich, 1,1-Dicyano-4-[4-(diethylamino)phenyl]buta-1,3-dienes: structure-property relationships, Eur. J. Org. Chem. 2012 (2012) 2756–2765, http://dx.doi.org/10.1002/ejoc.201200111.

[16] L. Zhang, D. Duan, Y. Liu, C. Ge, X. Cui, J. Sun, J. Fang, Highly selective off–on fluorescent probe for imaging thioredoxin reductase in living cells, J. Am. Chem. Soc. 136 (2014) 226–233, http://dx.doi.org/10.1021/ja408792k.

[17] Pavel A. Panchenko, Antonina N. Arkhipova, Olga A. Fedorova, Yuri V. Fedorov, Marina A. Zakharko, Jonusauskas Gediminas, Controlling photophysics of styrylnaphthalimides through TICT, fluorescence and E,Z-photoisomerization interplay, Phys. Chem. Chem. Phys. 19 (2017) 1244–1256, http://dx.doi.org/10.1039/c6cp07255k.

[18] L.K. Aschenbach, F.R. Knight, R.A.M. Randall, D.B. Cordes, A. Baggott, M. Bühl, A.M.Z. Slawin, J.D. Woollins, Onset of three-centre, four-electron bonding in peri-substituted acenaphthenes: a structural and computational investigation, Dalton Trans. 41 (2012) 3141–3153, http://dx.doi.org/10.1039/C1DT11697E.

[19] P. Alaei, S. Rouhani, K. Gharanjig, J. Ghasemi, A new polymerizable fluorescent PET chemosensor of fluoride (F-) based on naphthalimide-thiourea dye, Spectrochim. Acta Part A Mol. Biomol. Spectrosc. 90 (2012) 85–92, http://dx.doi.org/10.1016/j.saa.2012.01.008.

[20] T.A. Alhujran, L.N. Dawe, P.E. Georghiou, Synthesis of functionalized acenaphthenes and a new class of homooxacalixarenes, Org. Lett. 14 (2012) 3530–3533, http://dx.doi.org/10.1021/ol301538s.

[21] H.W.W. Ehrlich, A refinement of the crystal and molecular structure of acenaphthene, Acta Crystallogr. 10 (1957) 699–705, http://dx.doi.org/10.1107/S0365110X5700242X.

[22] Chao Xu, Wen-Feng Luo, Li-Jun Li, Synthesis and enantiomer separation of 5-(1-(3,5-dinitrobenzoylamino)pent-4-enyl)acenaphthene, Asian J. Chem. 22 (2010) 3923–3928, http://dx.doi.org/10.1016/j.tetasy.2009.01.015.

[23] M. Kumar, S. Roy, M.S.H. Faizi, S. Kumar, M.K. Singh, S. Kishor, S.C. Peter, R.P. John, Synthesis, crystal structure and luminescence properties of acenaphthene benzohydrazide based ligand and its zinc(II) complex, J. Mol. Struct. 1128 (2017) 195–204, http://dx.doi.org/10.1016/J.MOLSTRUC.2016.08.004.

[24] M.P. Cava, K.E. Merkel, R.H. Schlessinger, Pleiadene systems-II : on the mechanism of acepleiadylene formation - a vinylogous elimination in the acenaphthene series, Tetrahedron 21 (1965) 3059–3064, http://dx.doi.org/10.1016/S0040-4020(01)96925-X.

[25] G. Felix, M. Laguerre, J. Dunogues, R. Calas, Synthesis of new functional acenaphthylene derivatives. 2. Regioselective electrophilic substitution of silylated acenaphthenes and acenaphthylenes, J. Org. Chem. 47 (1982) 1423–1427, http://dx.doi.org/10.1021/jo00347a008.

[26] D.A. Evans, L.M. Lee, I. Vargas-Baca, A.H. Cowley, Photophysical tuning of the aggregation-induced emission of a series of para-substituted aryl bis(imino)acenaphthene zinc complexes, Dalton Trans. 44 (2015) 11984–11996, http://dx.doi.org/10.1039/C5DT01529D.

[27] D.A. Evans, L.M. Lee, I. Vargas-Baca, A.H. Cowley, Aggregation-induced emission of bis(imino)acenaphthene zinc complexes: photophysical tuning via methylation of the flanking aryl substituents, Organometallics 34 (2015) 2422–2428, http://dx.doi.org/10.1021/om501191c.

[28] P. Majumdar, J. Mack, T. Nyokong, Synthesis, characterization and photophysical properties of an acenaphthalene fused-ring-expanded NIR absorbing aza-BODIPY dye, RSC Adv. 5 (2015) 78253–78258, http://dx.doi.org/10.1039/C5RA14916A.

[29] L. Liu, C. Zhang, J. Zhao, The effect of the regioisomeric naphthalimide acetylide ligands on the photophysical properties of N^N Pt(ii) bisacetylide complexes, Dalton Trans. 43 (2014) 13434, http://dx.doi.org/10.1039/C4DT01732C.

[30] A.D. Kitchin, S. Velate, M. Chen, K.P. Ghiggino, T.A. Smith, R.P. Steer, Photophysics of a dithioester RAFT polymerization agent and the acenaphthenyl model light-harvesting chromophore, Photochem. Photobiol. Sci. 6 (2007) 853, http://dx.doi.org/10.1039/b702811c.

[31] U. El-Ayaan, A.A.M. Abdel-Aziz, S. Al-Shihry, Solvatochromism, DNA binding, antitumor activity and molecular modeling study of mixed-ligand copper(II) complexes containing the bulky ligand: Bis[N-(p-tolyl)imino]acenaphthene, Eur. J. Med. Chem. 42 (2007) 1325–1333, http://dx.doi.org/10.1016/j.ejmech.2007.02.014.

[32] M. Michalska, K. Grudzień, P. Małecki, K. Grela, Gold(I)-catalyzed formation of Naphthalene/Acenaphthene heterocyclic acetals, Org. Lett. 20 (2018) 954–957, http://dx.doi.org/10.1021/acs.orglett.7b03856.

[33] M. Shahid, S.S. Razi, P. Srivastava, R. Ali, B. Maiti, A. Misra, A useful scaffold based on acenaphthene exhibiting Cu2+ induced excimer fluorescence and sensing cyanide via Cu2+ displacement approach, Tetrahedron 68 (2012) 9076–9084, http://dx.doi.org/10.1016/j.tet.2012.08.052.

[34] L.A. Gifford, F.T.K. Owusu-Daaku, A.J. Stevens, Acenaphthene fluorescence derivatisation reagents for use in high-performance liquid chromatography, J. Chromatogr. A 715 (1995) 201–212, http://dx.doi.org/10.1016/0021-9673(95)00626-X.

[35] Y.M. Xie, Y. Deng, X.Y. Dai, J. Liu, L. Ouyang, Y.Q. Wei, Y.L. Zhao, Synthesis and biological evaluation of novel acenaphthene derivatives as potential antitumor agents, Molecules 16 (2011) 2519–2526, http://dx.doi.org/10.3390/molecules16032519.

[36] M.J. Frisch, G.W. Trucks, H.B. Schlegel, G.E. Scuseria, M.A. Robb, J.R. Cheeseman, G. Scalmani, V. Barone, G.A. Petersson, H. Nakatsuji, X. Li, M. Caricato, A. Marenich, J. Bloino, B.G. Janesko, R. Gomperts, B. Mennucci, H.P. Hratchian, J.V. Ortiz, A.F. Izmaylov, J.L. Sonnenberg, D. Williams-Young, F. Ding, F. Lipparini, F. Egidi, J. Goings, B. Peng, A. Petrone, T. Henderson, D. Ranasinghe, V.G. Zakrzewski, N.R.J. Gao, G. Zheng, W. Liang, M. Hada, M. Ehara, K. Toyota, R. Fukuda, J. Hasegawa, M. Ishida, T. Nakajima, Y. Honda, O. Kitao, H. Nakai,

T. Vreven, K. Throssell, J.A.J. Montgomery, J.E. Peralta, F. Ogliaro, M. Bearpark, J.J. Heyd, E. Brothers, K.N. Kudin, V.N. Staroverov, T. Keith, R. Kobayashi, J. Normand, K. Raghavachari, A. Rendell, J.C. Burant, S.S. Iyengar, J. Tomasi, M. Cossi, J.M. Millam, M. Klene, C. Adamo, R. Cammi, J.W. Ochterski, R.L. Martin, K. Morokuma, O. Farkas, J.B. Foresman, D.J. Fox, Gaussian 09, Revision C.01. Gaussian, Inc, Gaussian 09, Revis. B.01, Gaussian, Inc., Wallingford CT., 2010.

[37] P.J. Stephens, F.J. Devlin, C.F. Chabalowski, M.J. Frisch, Ab Initio calculation of vibrational absorption and circular dichroism spectra using density functional force fields, J. Phys. Chem. 98 (1994) 11623–11627, http://dx.doi.org/10.1021/j100096a001.

[38] A.D. Becke, Density-functional exchange-energy approximation with correct asymptotic behavior, Phys. Rev. A 38 (1988) 3098–3100, http://dx.doi.org/10.1103/PhysRevA.38.3098.

[39] A.D. Becke, A new mixing of Hartree–Fock and local density-functional theories, J. Chem. Phys. 98 (1993) 1372–1377, http://dx.doi.org/10.1063/1.464304.

[40] C. Lee, W. Yang, R.G. Parr, Development of the colle-salvetti correlation-energy formula into a functional of the electron density, Phys. Rev. B 37 (1988) 785–789, http://dx.doi.org/10.1103/PhysRevB.37.785.

[41] G. Saranya, P. Kolandaivel, K. Senthilkumar, Optical absorption and emission properties of fluoranthene, benzo[*k*]fluoranthene, and their derivatives. A DFT Study, J. Phys. Chem. A 115 (2011) 14647–14656, http://dx.doi.org/10.1021/jp208617s.

[42] A.D. Laurent, D. Jacquemin, TD-DFT benchmarks: a review, Int. J. Quantum Chem. 113 (2013) 2019–2039, http://dx.doi.org/10.1002/qua.24438.

[43] Y. Houari, S. Chibani, D. Jacquemin, A.D. Laurent, TD-DFT assessment of the excited state intramolecular proton transfer in hydroxyphenylbenzimidazole (HBI) dyes, J. Phys. Chem. B 119 (2015) 2180–2192, http://dx.doi.org/10.1021/jp505036d.

[44] E. Cancès, B. Mennucci, J. Tomasi, A new integral equation formalism for the polarizable continuum model: theoretical background and applications to isotropic and anisotropic dielectrics, J. Chem. Phys. 107 (1997) 3032, http://dx.doi.org/10.1063/1.474659.

[45] H. Heitele, P. Finckh, M.E. Michel-Beyerle, Synthesis of a rigid electron-donor/acceptor compound-evidence for intramolecular charge separation, Angew. Chemie Int. Ed. Engl. 28 (1989) 619–620, http://dx.doi.org/10.1002/anie.198906191.

[46] A. Szłapa, S. Kula, U. Błaszkiewicz, M. Grucela, E. Schab-Balcerzak, M. Filapek, Simple donor-π-acceptor derivatives exhibiting aggregation-induced emission characteristics for use as emitting layer in OLED, Dye Pigm. 129 (2016) 80–89, http://dx.doi.org/10.1016/j.dyepig.2016.02.002.

[47] J. Zhang, W. Chen, S. Kalytchuk, K.F. Li, R. Chen, C. Adachi, Z. Chen, A.L. Rogach, G. Zhu, P.K.N. Yu, W. Zhang, K.W. Cheah, X. Zhang, C.S. Lee, Self-assembly of electron donor-acceptor-based carbazole derivatives: novel fluorescent organic nanoprobes for both one- and two-photon cellular imaging, ACS Appl. Mater. Interfaces 8 (2016) 11355–11365, http://dx.doi.org/10.1021/acsami.6b03259.

[48] R. Kurata, A. Ito, M. Gon, K. Tanaka, Y. Chujo, Diarylamino- and diarylboryl-substituted donor-acceptor pyrene derivatives: influence of substitution pattern on their photophysical properties, J. Org. Chem. 82 (2017) 5111–5121, http://dx.doi.org/10.1021/acs.joc.7b00315.

[49] V.D. Gupta, A.B. Tathe, V.S. Padalkar, V.S. Patil, K.R. Phatangare, P.G. Umape, P. Ramasami, N. Sekar, TDDFT investigation of the electronic structures and photophysical properties of fluorescent extended styryl push-pull chromophores containing carbazole unit, J. Fluoresc. 23 (2013) 1121–1138, http://dx.doi.org/10.1007/s10895-013-1241-7.

[50] V.D. Gupta, A.B. Tathe, V.S. Padalkar, P.G. Umape, N. Sekar, Red emitting solid state fluorescent triphenylamine dyes: synthesis, photo-physical property and DFT study, Dye Pigm. 97 (2013) 429–439, http://dx.doi.org/10.1016/j.dyepig.2012.12.024.

[51] R.D. Telore, M.A. Satam, N. Sekar, NLOphoric studies in thiazole containing symmetrical push-pull fluorophores - combined experimental and DFT approach, Opt. Mater. (Amst.) 48 (2015) 271–280, http://dx.doi.org/10.1016/j.optmat.2015.08.006.

[52] K.G. Thorat, N. Sekar, Pyrrole-thiazole based push-pull chromophores: an experimental and theoretical approach to structural, spectroscopic and NLO properties of the novel styryl dyes, J. Photochem. Photobiol. A Chem. 333 (2017) 1–17, http://dx.doi.org/10.1016/j.jphotochem.2016.10.009.

[53] S.K. Lanke, N. Sekar, Novel NLOphoric carbazole-based push pull chromophores: synthesis, photophysical properties and TD-DFT study, J. Photochem. Photobiol. A Chem. 321 (2016) 63–71, http://dx.doi.org/10.1016/j.jphotochem.2016.01.014.

[54] S.B. Chemate, N. Sekar, Novel iminocoumarin derivatives: synthesis, spectroscopic and computational studies, J. Fluoresc. 25 (2015) 1615–1628, http://dx.doi.org/10.1007/s10895-015-1648-4.

[55] X. Liu, Z. Xu, J.M. Cole, Molecular design of UV − vis absorption and emission properties in organic fluorophores : toward larger bathochromic shifts, enhanced molar extinction coe ffi cients, and Greater stokes shifts, J. Phys. Chem. C 117 (2013) 16584–16595, http://dx.doi.org/10.1021/jp404170w.

[56] M. Crane, D. Boga, 1,1-dicyano-4-[4-(diethylamino)phenyl]buta-1,3-dienes: Structure–Property relationships, Eur. J. Org. Chem. (2012) 2756–2765, http://dx.doi.org/10.1002/ejoc.201200111.

[57] M. Blanchard-Desce, V. Alain, L. Midrier, R. Wortmann, S. Lebus, C. Glania, P. Krämer, A. Fort, J. Muller, M. Barzoukas, Intramolecular charge transfer and enhanced quadratic optical non-linearities in push pull polyenes, J. Photochem. Photobiol. A Chem. 105 (1997) 115–121, http://dx.doi.org/10.1016/S1010-6030(96)04547-9.

[58] J.L. Oudar, D.S. Chemla, Hyperpolarizabilities of the nitroanilines and their relations to the excited state dipole moment, J. Chem. Phys. 66 (1977) 2664–2668, http://dx.doi.org/10.1063/1.434213.

[59] A. Sena, V. Krishnana, Spectroscopic, redox and photophysical properties of push–pull fluoroarylporphyrins, J. Chem. Soc. Faraday Trans. 93 (1997) 4281–4288, http://dx.doi.org/10.1039/A704663D.

[60] N. Mataga, Y. Kaifu, M. Koizumi, Solvent effects upon fluorescence spectra and the dipolemoments of excited molecules, Bull. Chem. Soc. Jpn. 29 (1956) 465–470, http://dx.doi.org/10.1246/bcsj.29.465.

[61] E.G. McRae, Theory of solvent effects on molecular electronic spectra. Frequency shifts, J. Phys. Chem. 61 (1957) 562–572, http://dx.doi.org/10.1021/j150551a012.

[62] H. Beens, H. Knibbe, A. Weller, Dipolar nature of molecular complexes formed in the excited state, J. Chem. Phys. 47 (1967) 1183–1184, http://dx.doi.org/10.1063/1.1712006.

[63] E. Lippert, W. Rettig, V. Bonacickoutecky, F. Heisel, J.A. Miehe, Photophysics of internal twisting, Adv. Chem. Phys. 68 (1987) 1–173, http://dx.doi.org/10.1002/9780470142967.ch1.

[64] Z.R. Grabowski, K. Rotkiewicz, W. Rettig, Structural changes accompanying intramolecular electron transfer: focus on twisted intramolecular charge-transfer states and structures, Chem. Rev. 103 (2003) 3899–4031, http://dx.doi.org/10.1021/cr940745l.

[65] D.A. Kleinman, Nonlinear dielectric polarization in optical media, Phys. Rev. 126 (1962) 1977–1979, http://dx.doi.org/10.1103/PhysRev.126.1977.

[66] A. Kawski, P. Bojarski, Comments on the determination of excited state dipole moment of molecules using the method of solvatochromism, Spectrochim. Acta Part A Mol. Biomol. Spectrosc. 82 (2011) 527–528, http://dx.doi.org/10.1016/j.saa.2011.05.102.

[67] S. Kothavale, N. Sekar, A new type of triphenylamine based coumarin–rhodamine hybrid compound: synthesis, photophysical properties, viscosity sensitivity and energy transfer, RSC Adv. 6 (2016) 105387–105397, http://dx.doi.org/10.1039/C6RA24485H.

[68] M.A. Haidekker, T.P. Brady, D. Lichlyter, E.A. Theodorakis, Effects of solvent polarity and solvent viscosity on the fluorescent properties of molecular rotors and related probes, Bioorg. Chem. 33 (2005) 415–425, http://dx.doi.org/10.1016/j.bioorg.2005.07.005.

[69] D.M. de Leeuw, M.M.J. Simenon, A.R. Brown, R.E.F. Einerhand, Stability of n-type doped conducting polymers and consequences for polymeric microelectronic devices, Synth. Met. 87 (1997) 53–59, http://dx.doi.org/10.1016/S0379-6779(97)80097-5.

[70] J. Wang, X. Chen, G. Zhang, Z. Liu, D. Zhang, Conjugated electron donor–acceptor molecules with (E)-[4,4′-biimidazolylidene]-5,5′(1H,1′H)-dione for new organic semiconductors, J. Mater. Chem. C 2 (2014) 1149, http://dx.doi.org/10.1039/c3tc31741b.

[72] D.R. Mohbiya, N. Sekar, Tuning 'Stokes shift' and ICT character by varying the donor group in imidazo[1,5 A]pyridines: a combined optical, DFT, TD-DFT and NLO approach, Chem. Select 3 (2018) 1635–1644, http://dx.doi.org/10.1002/slct.201702579.

[73] W.-R. Wu, Theoretical investigation on the excited-state intramolecular proton transfer mechanism of 2-(2′-benzofuryl)-3-hydroxychromone, J. Phys. Org. Chem. 28 (2015) 596–601, http://dx.doi.org/10.1002/poc.3455.

[74] C. Tabti, N. Benhalima, Molecular structure, vibrational assignments and non-linear optical properties of by DFT and ab initio HF calculations, Adv. Mater. Phys. Chem. 5 (2015) 221–228.

[75] C. Adant, M. Dupuis, J.L. Bredas, Ab Initio study of the nonlinear optical properties of urea: electron correlation and dispersion effects, Int. J. Quantum Chem. 56 (1995) 497–507, http://dx.doi.org/10.1002/qua.560560853.

[76] F. Momicchioli, G. Ponterini, D. Vanossi, First- and second-order polarizabilities of simple merocyanines. An experimental and theoretical reassessment of the two-level model, J. Phys. Chem. A 112 (2008) 11861–11872, http://dx.doi.org/10.1021/jp8080854.

[77] U. Warde, N. Sekar, NLOphoric mono-azo dyes with negative solvatochromism and in-built ESIPT unit from ethyl 1,3-dihydroxy-2-naphthoate: estimation of excited state dipole moment and pH study, Dye Pigm. 137 (2017) 384–394, http://dx.doi.org/10.1016/j.dyepig.2016.10.032.

[78] S.N. Margar, L. Rhyman, P. Ramasami, N. Sekar, Fluorescent difluoroboron-curcumin analogs: an investigation of the electronic structures and photophysical properties, Spectrochim. Acta Part A Mol. Biomol. Spectrosc. 152 (2016) 241–251, http://dx.doi.org/10.1016/j.saa.2015.07.064.

[79] M.R. Shreykar, N. Sekar, Coumarin-Rhodamine hybrids - synthesis, photophysical properties, NLO properties and DFT studies, Chem. Select 2 (2017) 1464–1478, http://dx.doi.org/10.1002/slct.201601879.

[80] K.C. Avhad, D.S. Patil, S. Chitrambalam, M.C. Sreenath, I.H. Joe, N. Sekar, Viscosity induced emission of red-emitting NLOphoric coumarin morpholine-thiazole hybrid styryl dyes as FMRs: consolidated experimental and theoretical approach, Opt. Mater. (Amst). 79 (2018) 90–107, http://dx.doi.org/10.1016/j.optmat.2018.03.024.

[81] B. Carlotti, R. Flamini, I. Kikaš, U. Mazzucato, a. Spalletti, Intramolecular charge transfer, solvatochromism and hyperpolarizability of compounds bearing ethenylene or ethynylene bridges, Chem. Phys. 407 (2012) 9–19, http://dx.doi.org/10.1016/j.chemphys.2012.08.006.

[82] J. Liu, W. Gao, I.V. Kityk, X. Liu, Z. Zhen, Optimization of polycyclic electron-donors based on julolidinyl structure in push-pull chromophores for second order NLO effects, Dye Pigm. 122 (2015) 74–84, http://dx.doi.org/10.1016/j.dyepig.2015.06.007.

[83] C.W. Dirk, L.T. Cheng, M.G. Kuzyk, A simplified three-level model describing the molecular third-order nonlinear optical susceptibility, Int. J. Quantum Chem. 43 (1992) 27–36, http://dx.doi.org/10.1002/qua.560430106.

[84] M.G. Kuzyk, C.W. Dirk, Effects of centrosymmetry on the nonresonant electronic third-order nonlinear optical susceptibility, Phys. Rev. A 41 (1990) 5098–5109, http://dx.doi.org/10.1103/PhysRevA.41.5098.

[85] S. Deckers, S. Vandendriessche, D. Cornelis, F. Monnaie, G. Koeckelberghs, I. Asselberghs, T. Verbiest, M.A. Van Der Veen, Poly(3-alkylthiophene)s show unexpected second-order nonlinear optical response, Chem. Commun. 50 (2014) 2741–2743, http://dx.doi.org/10.1039/c3cc48099b.

[86] F. Meyers, S.R. Marder, B.M. Pierce, J.L. Bredas, Electric field moldulated nonlinear optical properties of donor-acceptor polyenes: sum-over-states investigation of the relationship between molecular polarizabilities (α, β, and γ) and bond length alteration, J. Am. Chem. Soc. 116 (1994) 10703–10714, http://dx.doi.org/10.1021/ja00102a040.

[87] A.E. Stiegman, E. Graham, K.J. Perry, L.R. Khundkar, L.T. Cheng, J.W. Perry, The electronic structure and second-order nonlinear optical properties of donor-acceptor acetylenes: a detailed investigation of structure-property relationships, J. Am. Chem. Soc. 113 (1991) 7658–7666, http://dx.doi.org/10.1021/ja00020a030.